Thermal and Flow Property–Morphology Relationship of Sugarcane Bagasse Fiber-Filled Polyamide 6 Blends

R. Dweiri, C. H. Azhari

Department of Mechanical and Materials Engineering, Faculty of Engineering, Universiti Kebangsaan Malaysia, 43600 Bangi, Malaysia

Received 18 June 2003; accepted 21 January 2004

ABSTRACT: The structure–property relationship of sugarcane bagasse fiber-filled polyamide 6 blends at different blend compositions has been investigated. Blends were prepared in the composition of wt % PA6/wt % bagasse as follows: 98/2, 95/5, and 90/10 for three fiber length ranges (<100, <250, and <500 μm) using a twin-screw extruder. Thermal properties were evaluated by measuring the glass transition temperature T_g, enthalpy of fusion ΔH_f, crystallinity X_c and thermogravimetry, TG. Results showed that T_g of the composites changed with change in fiber loading and length. The X_c as well as ΔH_f of the blends reduced to almost half its value for the neat PA6. The thermogravimetric curves TG showed that the thermal stability of the composites was lower than that of the neat PA6. Rheological properties were studied as a function of fiber loading, fiber length, shear rate, and temperature. The viscosity of composites increased with increasing fiber loading and length at low shear rates but decreased below that of neat PA6 at high shear rates. It was also found to be temperature sensitive, and influenced by fiber lengths particularly at higher temperatures. The morphology of the blends was studied using a Leica laser scanning confocal microscopy at two different regions: at the wall, and the core. The micrographs of the blends showed that fibers present in the form of bundles were found at the wall of the extrudates and increased in volume with increase in both length and concentration, at the same temperature and shear stress. In the core region, there is laminar flow, presenting striation morphology, with the omnipresent bundles of fibers dispersed in the matrix. At higher shear rates, the bundles were pushed to the wall.
 J Appl Polym Sci 92: 3744–3754, 2004

Key words: thermal properties; morphology; polyamides; fillers

INTRODUCTION

In recent years, natural fiber composites have emerged as a realistic alternative to wood-filled and glass-reinforced composites. Using natural fibers such as lignocellulosics in the production of thermoplastic composites has achieved cost reduction, improved mechanical properties, and ease of processibility even when using conventional polymer processing machinery.[1–3] This development has been brought about due to the advantages offered by lingocellulosic fillers over their inorganic counterparts when used as reinforcement. Such advantages include lower densities, greater deformability, less abrasiveness to expensive molds, and mixing equipment, and lower material cost. Moreover, lignocellulosic-based fillers are derived from renewable resources. Despite these advantages, the major drawback associated with the use of natural fibers as reinforcement in thermoplastics is the lowering of processing temperature due to the possibility of lignocellulosic degradation as well as the possibility of volatile emissions that could affect composite properties. Another disadvantage of using natural fibers as reinforcement is their hydrophilic nature, causing reduced compatibility between the fiber and the matrix, leading to the degradation of mechanical properties of the natural fiber-reinforced composites. This disadvantage has been overcome by the pretreatment of the fibers, either by physical or chemical means.

Studies on plastics reinforced with natural fibers such as jute, sisal, coir, pineapple, bamboo, oil palm empty fruit bunch (the remaining material after the palm oil kernels have been harvested) kenaf, coconut, and hemp have been reported by many researchers.[4–7] Compared to studies on natural fiber-reinforced composites, less effort has been focused on bagasse fiber-reinforced plastics. Sugarcane bagasse fibers are limited in their strength properties, but can compete in prices with other fibers such as sisal, jute, etc. Researchers such as Sayer[8] and Mclaughlin[9] have studied the strength of bagasse fiber-reinforced composites. Recently, researchers did reported research on the impact, tensile, and flexural mechanical behavior of sugarcane bagasse waste-reinforced EVA matrix composites[10,11] and also the bagasse fiber–polypropylene-based composites.[12] Some previous studies showed the possibility of using bagasse fiber into thermoplastic matrices by chemical modification by means of esterification[13] or cyanoethylation[14] before use. Atten-

Correspondence to: C. H. Azhari (mek@vlsi.eng.ukm.my).

Journal of Applied Polymer Science, Vol. 92, 3744–3754 (2004)

TABLE I
Physical Properties of PA6 and Bagasse

Physical property	PA6	Bagasse
Melt flow index MFI (g/10 min)	24	—
Tensile modulus E (GPa)	0.7	20 ± 2.5
Tensile strength σ (MPa)	55	2.7 ± 1.7
Elongation at break ε (%)	60	0.9
Melting temperature T_m (°C)	222	—
Softening temperature T_g (°C)	60	—
Density ρ (g/cc)	1.14	0.55
Cellulose content (%)		40
Lignin content (%)		15
Natural rubber content (%)		24.4

tion has also been given to the utilization of natural, chemically treated, and heat-treated sugar cane bagasse fibers to replace asbestos fibers in fiber-reinforced cement products.[15] Sugarcane bagasse was used also to reinforce thermoset polymers (phenolic and lignophenolic) to improve their low impact strength.[16]

Literature cites the use of typical plastics such as PE, PP, PS, PVC, as well as some elastic copolymers for blending with the lignocellulosics.[17–20] A few studies have focused on the use of natural fibers in engineering plastics such as polyamides and polycarbonates, particularly on aspects of the high melting temperatures of these polymers and the possibility of lignocellulosic degradation at these temperatures. PA is a strong and durable engineering thermoplastic, and for the past decade, it has been successfully reinforced by glass and carbon fibers and other inorganic reinforcements for use in sports, aerospace, and automotive applications.[21–23] Despite these advantages, PA suffers from the disadvantage of a narrow processing window, and has thus been incorporated into the PA/polyolefin blends to render them a larger processing one.[24–26] Much work on PA blends centered on PA/PP blends.[27–29] Blends of cellulose with PA prepared by a solution-coagulation method have also been studied.[30–33]

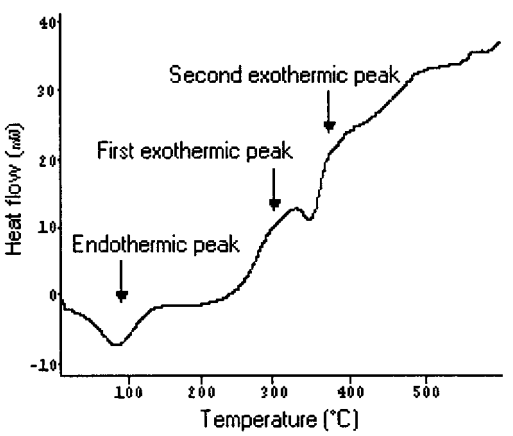

Figure 1 DSC thermogram of bagasse fiber.

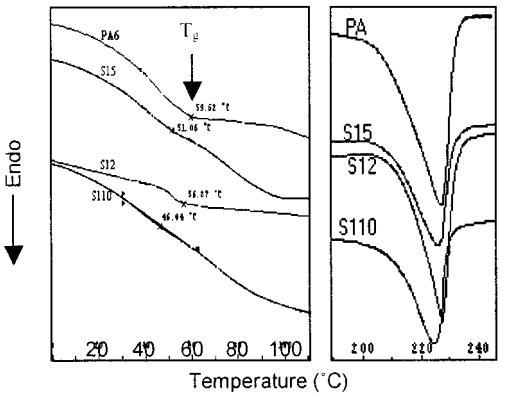

Figure 2 DSC thermograms of PA, S12, S15, and S110.

The aim of this work was to study the structure–property as well as the processing characteristics of bagasse/PA blends using differential scanning calorimetry (DSC), thermogravimetery (TG), and capillary rheometry, and to correlate the results to morphology. The effect of temperature, fiber loading, fiber length, and shear rate on the melt flow behavior of the composites were investigated, as this is very important because these could be related to the processability of the PA/bagasse blends when melt processed by techniques such as extrusion and injection molding. The flow behavior including flow orientation was correlated to the blend morphology.

EXPERIMENTAL

Polyamide 6 Bayer (Durethan B40 ECS) was supplied by Bayer Sdn. Bhd., and it was used in the as-received state. The bagasse was soaked in water for 24 h then refined using the refiner mechanical pulp machine in Forest Research Institute of Malaysia (FRIM), which was further air dried for 72 h. This was sieved accord-

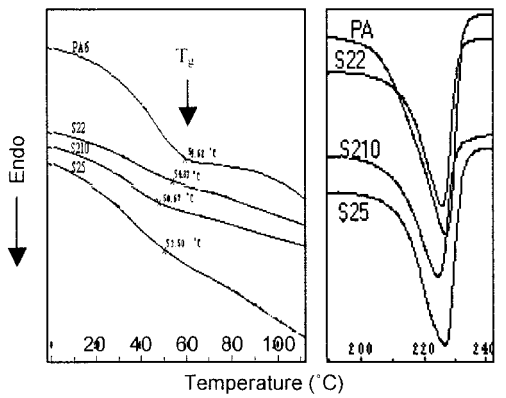

Figure 3 DSC thermograms of PA, S22, S25, and S210.

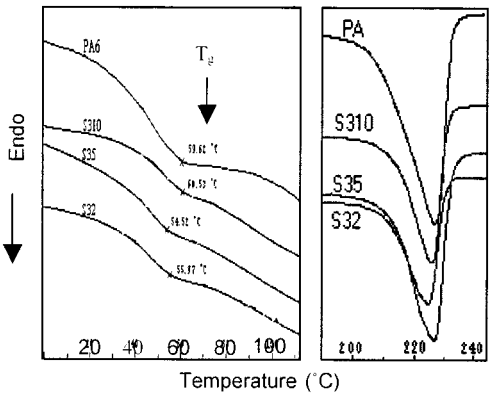

Figure 4 DSC thermograms of PA, S32, S35, and S310.

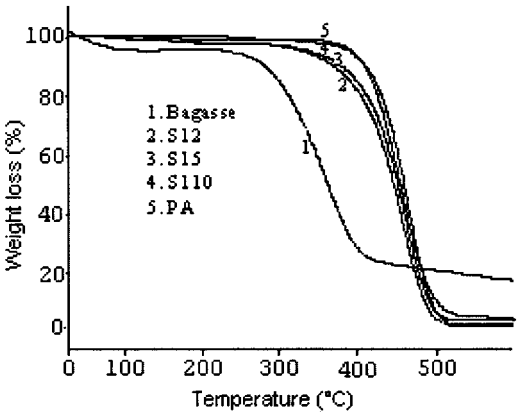

Figure 5 TG thermograms of bagasse, PA, S12, S15, and S110.

ing to fractions given the designation L1 <100, L2 <250, and L3 <500 μm. The bagasse fibers were evaluated for size using an optical microscope (Olympus 1000). Table I gives the physical properties of PA and bagasse fiber.

The fibers and the PA were dried in an oven at 70°C for 24 h. They were then blended in an intermeshing counterrotating, twin-screw extruder (Rheomex CTW100p) at a temperature of 210°C. The screw speed was maintained at 60 rpm. The extrudates were then ground into small pellets. Blends were prepared containing 2, 5, and 10 wt % of bagasse fiber of lengths L1, L2, and L3 and denoted as: sample, fiber length, weight percentage. Samples prepared had these notations, S12, S15, S110, S22, S25, S210, S32, S35, and S310.

The thermal behavior of bagasse, PA6, and the blends were studied by means of differential scanning calorimetry (DSC) and thermogravimetry (TGA). In DSC, a Mettler, Toledo DSC (DEMO version) is used to determine melting points (T_m), glass transition temperature (T_g), and enthalpy of fusion (ΔH). The specimens were scanned from −20 to 260°C at a heating rate of 10°C/min in the presence of nitrogen. For bagasse, the specimen was scanned from room temperature to 600°C. In TGA, the specimens were scanned from 25 to 600°C at a heating rate of 20°C/min in the presence of nitrogen using a Mettler, Toledo TGA (TGA 851E).

Rheological measurements were carried out using a Shimadzu CFT-500D capillary rheometer, with JIS K7210 as the reference standard. A die of 10 mm length and 1 mm diameter was used. Measurements were made at three shear stresses, 184, 368, and 490 KPa and three temperatures of 230, 240, and 250°C. The results obtained were expressed as, η, apparent viscosity, γ, apparent shear rate and τ, apparent shear stress. The apparent shear rate, γ, was calculated using the following equation:

$$\gamma = \frac{32Q}{\pi D^3} \cdot 10^3 (\mathrm{s}^{-1}) \quad (1)$$

where D is the die orifice diameter (mm).

TABLE II
Thermal Properties of PA6 and PA/Bagasse Blends From DSC

Sample	T_g °C	T_m °C	ΔH_f[a] Jg	X_c %
PA6	59.6	225.8	103.1	44.8
S12	56.7	225.3	47.5	21.1
S15	50.7	224.5	42.5	19.4
S110	46.0	223.6	38.4	18.5
S22	54.8	225.0	49.4	22.0
S25	53.5	225.2	44.3	20.3
S210	50.7	223.5	45.1	21.8
S32	56.0	225.7	48.4	21.5
S35	54.5	224.8	42.7	19.5
S310	60.5	224.0	46.9	22.6

[a] ΔH_f is determined from the area of the melting peak.

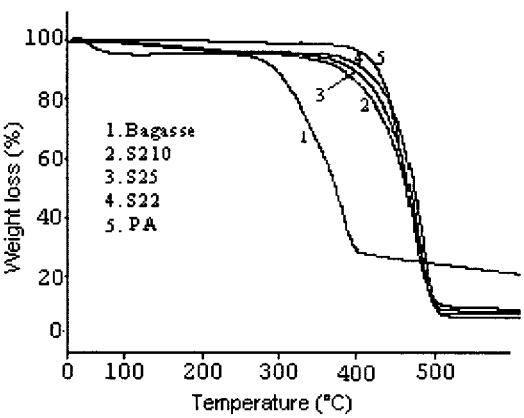

Figure 6 TG thermograms of bagasse, PA, S22, S25, and S210.

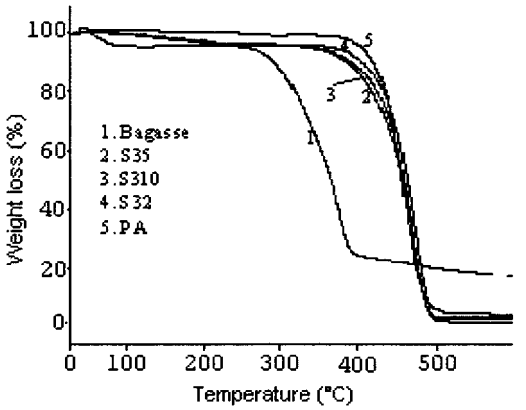

Figure 7 TG thermograms of bagasse, PA, S32, S35, and S310.

The apparent shear stress, τ, was calculated using the following equation;

$$\tau = \frac{PD}{4L}(\text{Pa}) \tag{2}$$

where P is the test pressure (Pa), and L is the die length (mm).

The apparent viscosity, η, was calculated using the following equation;

$$\eta = \frac{\tau}{\gamma} = \frac{\pi D^4 P}{128LQ} \times 10^{-3}\ (\text{Pa·s}) \tag{3}$$

$$Q = A \cdot \frac{S_2 - S_1}{10 \cdot \Delta t}(\text{cm}^3/\text{s}) \tag{4}$$

where A is the piston cross sectional area (cm^3), S_1 is the calculation start point (mm), S_2 is the calculation end point (mm), and Δt is the time for the piston to travel from S_1 to S_2 (second).

The morphology of the blends was observed using a Leica (Leica DMLM 1000) laser scanning confocal microscopy. The blends need no prior preparation before observation. Micrographs were obtained at the magnification of 350 times and at two different regions: the periphery (i.e., near the wall) and at the core (i.e., middle of the channel).

RESULTS AND DISCUSSION

Thermal properties

Differential scanning calorimetry (DSC)

The DSC technique was used to determine the reduction in the crystallinity and thermal decomposition of the bagasse fiber. The thermogram of the fiber is as illustrated in Figure 1. The DSC thermogram showed an endothermic peak at about 98.71°C that could be due to the natural lattices present in the bagasse. It also showed two exothermic peaks at around 320 and 377°C. The first exothermic peak was used to assess the thermal degradation of crystallites in bagasse fibers, following the work of Mkwaimbo et al.[34]

The thermal parameters; T_m, T_g, ΔH_f, and X_c were determined and calculated from the DSC thermograms of PA/bagasse blends (Figs. 2, 3, and 4) and summarized in Table II. The percentage crystallinity (X_c) of PA6 phase in the blends was calculated from the following equation:

$$X_c(\%\text{crystallinity}) = \left(\frac{\Delta H_f}{\Delta \cdot H_f^0}\right) \cdot \left(\frac{100}{w}\right) \tag{5}$$

where $\Delta H^\circ_f = 230.12\ \text{J g}^{-1}$ is the fusion enthalpy of completely crystalline PA6,[35] and w is the weight fraction of PA6 in the blends.

It can be noticed that a melting point depression of about 2°C occurred at the blend composition of 10% bagasse fiber. This depression in the melting peak temperature of PA6 in the blends could be attributed to a partial miscibility of bagasse fiber in the amorphous phase of PA that might have occurred. An alternative explanation is that it could have been due to changes in the crystal structure of PA (i.e., changes in either the crystallite size or crystal dimensions). The depression of the melting temperature is also an indication of strong physical interfacial interactions between bagasse fiber and PA as observed by other researchers.[30–33]

The glass transition temperature (T_g) of the blends was found to change with the change in fiber loading and fiber length. The T_g of PA6 was estimated at 59.6°C. At the 10% bagasse content, the T_g of PA6 shifted to the lower temperatures of 46.0 and 50.7°C for blends containing <100 and <250 μm fibers, re-

TABLE III
Percentage Weight Loss of PA/Bagasse Blends at Different Temperatures

	Weight loss (%)					
Sample	100°C	200°C	300°C	400°C	450°C	500°C
Bagasse	4.21	4.48	14.78	75.53	77.74	79.58
PA6	0.43	0.43	1.18	5.01	46.35	95.39
S12	0.39	0.47	0.92	6.75	47.87	97.69
S15	0.086	1.63	2.65	15.01	48.20	96.39
S110	0.21	1.53	2.66	17.50	52.06	94.70
S22	0.014	2.60	3.77	9.39	35.74	98.45
S25	0.42	3.20	4.05	12.9	43.36	97.57
S210	0.40	2.96	4.66	20.36	60.46	96.29
S32	0.22	2.94	3.88	11.57	50.78	98.43
S35	0.38	2.99	4.23	15.96	58.80	96.77
S310	0.55	3.39	4.178	13.60	52.38	97.43

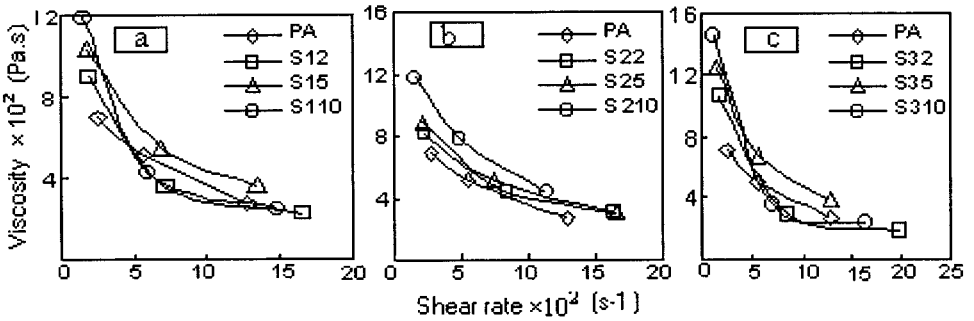

Figure 8 Viscosity vs shear rate at 230°C for (a) PA, S12, S15, and S110; (b) PA, S22, S25, and S210; (c) PA, S32, S35, and S310.

spectively. For blends containing <500 μm, the T_g shifted to a higher temperature of 60.5°C. The depression in T_g could be attributed to the plasticization effect of the fiber that has dissolved or diffused into the polymer.[2,36] Mention must be made that in the previous studies cited, the fibers were treated while that in our studies were not. Hence, the effect of chemical modification to plasticisization was not that significant. The increase of T_g observed in the blend S310 could be due to the effect of hampering the movement of the polymer molecule or chain due to the existence of flexible fibers in the matrix.[37]

PA6 is a highly crystalline material, and there was difficulty in determining its glass transition temperature using differential scanning calorimetry (DSC).

The DSC thermograms showed that the addition of bagasse fiber to PA resulted in a drastic decrease in ΔH_f to almost half the value of the matrix. The decrease of the ΔH_f observed could be attributed to the action of the fibers acting as a diluent in the PA6 matrix.[38] A comparison of X_c of the neat PA6 with the percentage of crystallinity calculated according to eq. (5) for the PA6 component in the blends showed that the crystallinity was reduced remarkably by incorporation of the fiber in the matrix. As reported in the previous study by Ramirez, the contributing factor could be that some PA6 regions have formed a mixture with the cellulose so as to hamper its crystallization, reducing crystalline regions in the final blend. This reduced the crystallinity values in the blends.

It can be noted that the decrease in T_g, ΔH_f, and X_c with the increase of fiber content was more pronounced for blends containing shorter fibers than those containing longer fibers. The ΔH_f and X_c were more or less the same at all fiber concentrations for blends containing fibers <250 and <500 μm, while they decreased in a regular manner for blends containing fibers <100 μm.

Thermogravimetry analysis (TGA)

Thermogravimetry plots (TG) for bagasse fiber, PA, and PA/bagasse blends are given in Figures 5, 6, and 7. Three temperature regions (45–80, 250–430, and those higher than 430°C) were considered when discussing the thermal stability of bagasse fibers. Between 80 and 250°C, the bagasse fibers were quite stable. At the first stage (45–80°C), a weight loss of 4.78% occurred, which could probably be due to the heat of vaporization of water in the sample; in other words, fiber dehydration occurred. A weight loss of 72.63% occurred at the second stage (250–430°C) that might be attributed to thermal depolymerization of hemicelluloses and the cleavage of glucosidic linkages of cellulose. The third weight loss of 22.59% started at about 430°C, which may be due to the further break-

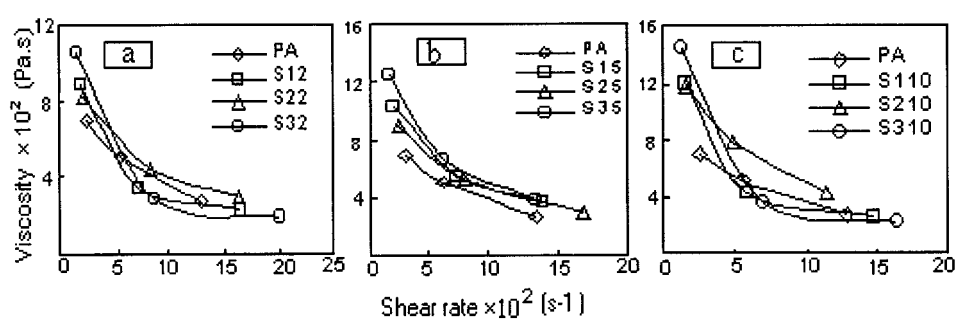

Figure 9 Viscosity vs shear rate at 230°C for (a) PA, S12, S22, and S32; (b) PA, S15, S25, and S35; (c) PA, S110, S210, and S310.

TABLE IV
Values of the Power Low Index (*n*) for PA/Bagasse Blends at 230°C

Sample	PA	S12	S15	S110	S22	S25	S210	S32	S35	S310
n value	0.39	0.33	0.49	0.29	0.50	0.48	0.50	0.28	0.46	0.26

age of the decomposition product of the second stage leading to the formation of tar through levoglucosan.[39–42]

In the case of PA, degradation was observed occurring in a single step. Up to the temperature of 350°C the sample was stable, and thereafter, a sharp weight loss occurred in the material. Degradation was completed at about 500°C, and during this stage the weight loss observed was 96%. About 4% residue remains above 500°C, and this indicated that the PA did not completely volatilize, leaving behind some ash.[43]

A step analysis of bagasse fiber, PA, and PA/bagasse blends was carried out, and the weight losses at different temperatures were given in Table III. As can be noticed from the table and the figures, the thermal stability of the blends was in the order of: (a) bagasse fiber < S110 < S15 < S12 < PA; (b) bagasse fiber < S210 < S25 < S22 < PA; (c) bagasse fiber < S35 < S310 < S32 < PA.

It can be observed from the results that the thermal stability of the PA/bagasse blends was lower than that of the neat PA, and it decreased with increasing fiber loading. Table III showed the same results as those from previous studies. It can be also noticed that blends tended to follow the profile of the neat PA more than the bagasse fiber, that is, at the 10% fiber loading the predominant behavior is thermoplastic.

The TG analysis indicated that bagasse fibers were thermally stable at the flow temperatures of PA, and as such, these fibers can be effectively used as reinforcement for such applications.

Rheological properties

Effect of fiber loading and shear rate on viscosity

Figure 8 showed the variation of melt viscosity of PA/bagasse blends with shear rate and fiber loading at 230°C. These curves were typical of pseudoplastic materials, which showed a decrease in viscosity with increasing shear rate. Such behavior was generally called "shear-thinning" behavior. All the systems investigated have been found to obey a power-law relationship in the shear rate range:

$$\eta_w = k(\gamma w)^{n-1} \tag{6}$$

where n is the power law index and k the consistency index.

It was clear from these curves that the viscosity of the blends increased with increase in the fiber loading at low shear rates. The viscosity decreased as the shear rate increased so that the increase in viscosity with fiber loading was more prominent at low shear rates compared to that at higher shear rates. However, at higher shear rates, the change in viscosity was marginal. The increase in viscosity of the composite was due to the fiber–fiber and fiber–matrix collisions. At low shear rates, the fibers were in a disoriented manner, and the probability of a fiber–fiber collision was much higher. This collision increased with fiber loading, and therefore, viscosity increased. As the shear rate increased, most of the shearing of the fiber took place close to the wall, and therefore, the fibers will strongly align along the axis. The probability of fiber–fiber collision was much less; hence, the increase in viscosity with fiber content was much less at higher shear rates.

Effect of fiber length on viscosity

The graphs of the melt viscosity vs shear rate and fiber length for PA/bagasse blends are as given in Figure 9(a)–(c). These curves are also typical of pseudoplastic materials and obeyed the power-law equation.

The curves above showed that, at low shear rates, blends containing <500-μm fibers showed the highest viscosity and blends containing fibers <250 μm

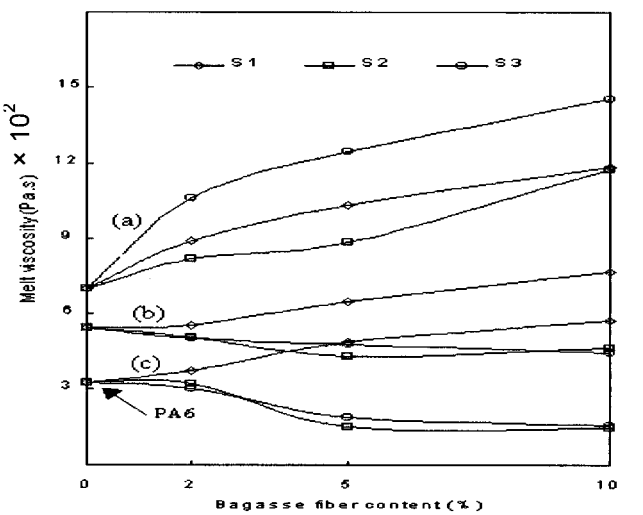

Figure 10 Melt viscosity vs bagasse fiber content for blends at (a) 230°C, (b) 240°C, (c) 250°C, and shear stress 184 KPa.

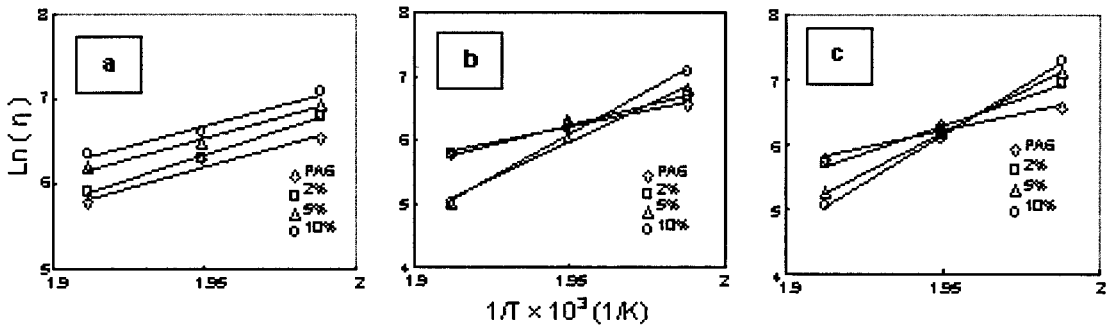

Figure 11 Ln (η) vs ($1/T$) at a constant shear stress of 184 KPa for (a) blends S1, (b) blends S2, (c) blends S3.

showed the lowest viscosity, while blends containing fibers < 100 μm fibers showed a viscosity intermediate to the two. The increase of viscosity of the composites on increasing fiber length was as expected, and comparable to previous studies[44] because at higher fiber lengths (i.e., the < 500 μm fibers in our case) it was difficult for the fibers to orient in the direction of flow. This was associated with the fiber entanglement at higher fiber loadings. Fibers having a shorter length (i.e., < 250 μm fibers) were more easily aligned along the direction of flow than longer fibers. For too short fibers, the chances for fiber orientation decreased and fiber–matrix interaction increased. This accounts for the higher values of viscosity in the case of composites containing < 100 μm fibers.

The values of the power law flow indices (n) of the power law relation: $\eta_w = k(\gamma_w)^{n-1}$ were obtained from the plots of η_w vs γ_w at a temperature of 230°C and tabulated in Table IV. The data was fitted to eq. (5) and determined the value of flow index.

The values of n for the PA and the blends were less than unity showing pseudoplastic nature of the melts. The n values of the blends varied with the variation in the fiber content and fiber length. About $\pm$30% deviation occurred in the n values compared to that of the neat PA, and no correlation of the results with the fiber length and fiber content can be established. Comparing blends containing 2% and 10% fiber content at different fiber lengths showed the same trend in the n values for both kind of blends. This is to say, that the n values were initially decreased then increased before it decreased again with the increase in fiber length. The decrease in the n value of some blends indicated more pseudoplasticity (i.e., more shear thinning behavior). The blends containing <500 μm fibers at 10% fiber content showed the lowest n value among the blends and the highest pseudoplasticity that might be due to the orientation of the fibers.[45]

Thus, the addition of fibers to a polymer influenced its viscosity and behaves like a reduction in the temperature of the melt, as both caused a rise in viscosity. This supports the idea that the enhanced viscosity was due to increased viscous energy dissipation in the matrix and that particle–particle interaction was not significant.[46]

It is now clear that the shear rates tested in the present study were not low enough to exhibit yield stress of the filled polymer. This yield stress is exhibited due to the formation of an interparticle network, which becomes quite strong at high filler loadings. Yield stress is most pronounced at very low shear rates, for example, 10^{-2} to 10^{0} s^{-1}, and very fine particle fillers. The finer the filler, the larger the ability of network formation and stronger the network exhibiting higher yield values.

TABLE V
Activation Energy of PA/Bagasse Blends

	Activation energy (J/mol)		
Sample code	2%	5%	10%
100% PA	—	85	—
S1	96	83	80
S2	103	194	227
S3	138	207	243

Effect of temperature

The effect of temperature on the viscosity of polymers is important as the polymers undergo considerable temperature changes during their processing. It is known that viscosity decreased with temperature for both filled and unfilled systems. At higher temperatures, molecular motion is accelerated due to the availability of greater free volume and also due to the decreasing entanglement density and weaker intermolecular interactions.[44]

Figure 10 showed the variation of melt viscosity with fiber loading for all kinds of blends at three different temperatures: 230, 240, and 250°C. The shear stress was kept constant at 184 KPa. At 230°C, the viscosity increased with increasing fiber length and blends containing < 500 μm fibers have the highest

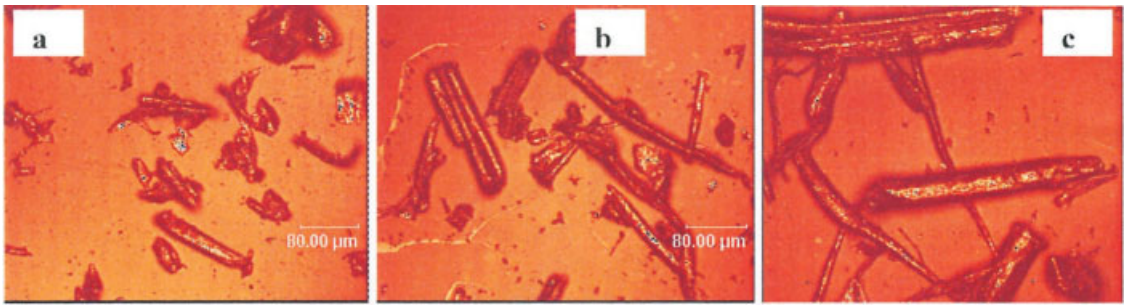

Figure 12 Micrographs of bagasse fiber of three different sizes: (a) L1 <100 μm, (b) L2 <250 μm, and (c) L3 <500 μm.

viscosity, while blends containing < 250 μm fibers have the lowest viscosity at all fiber concentration. This was discussed earlier. At 240°C, as well as 250°C, blends containing < 100 μm fibers showed viscosity higher than that of PA at all fiber concentration, while it was slightly lower than that of PA for blends containing < 250 μm fibers and blends containing < 500 μm fibers. This might be explained as follows: for short fibers, the viscosity was governed by fiber–matrix interaction that increased viscosity, while for longer fibers; it was governed by wall-slip that decreased the viscosity.

To further study the temperature dependence of viscosity of PA/bagasse blends, plots of Ln (η) vs ($1/T$) were plotted as shown in Figure 11. The shear stress was fixed at 184 KPa. Linear plots were obtained. The activation energy of the blends were calculated and tabulated in Table V from the slopes of these plots. The activation energy was obtained from the Arrhenius relationship:

$$\eta_0 = A \exp(E/RT) \tag{7}$$

where E is the activation energy, η_o is the zero-shear viscosity, A is the viscosity at $T = \infty$, R is the gas constant, and T is the absolute temperature. The higher the activation energy, the more temperature sensitive the material will be. So, blends containing (<500 μm) fibers at 10% bagasse showed the highest temperature sensitivity. The viscous flow of the blends increased with increasing fiber loading and fiber length. This indicated that the melt viscosity of the composites was more temperature sensitive than that of the nonfilled polymer.

Morphological properties

The morphology of the bagasse fibers according to size are as depicted in Figure 12. The bagasse fibers were shown to be rod-like particles with diameters of about 10 μm. The sizing was made on the basis of the length of the fibers because sieving them into fractions would be to separate on the basis of lengths and not diameters.

The blend morphology of the PA showed the matrix to be smooth with a lamellar-like structure. These may be looked at in detail in Figure 13.

Bagasse fiber was found to have a strong tendency to exist in the form of fiber bundles throughout the cross-section of the extrudates. Ishak and coworkers have reported the same phenomenon in their investigation on the mechanical properties of oil palm empty fruit bunch (EFB)-filled HDPE composites.[7] The fibers in bundles were found at the wall, and increased in volume with an increase in both length and concen-

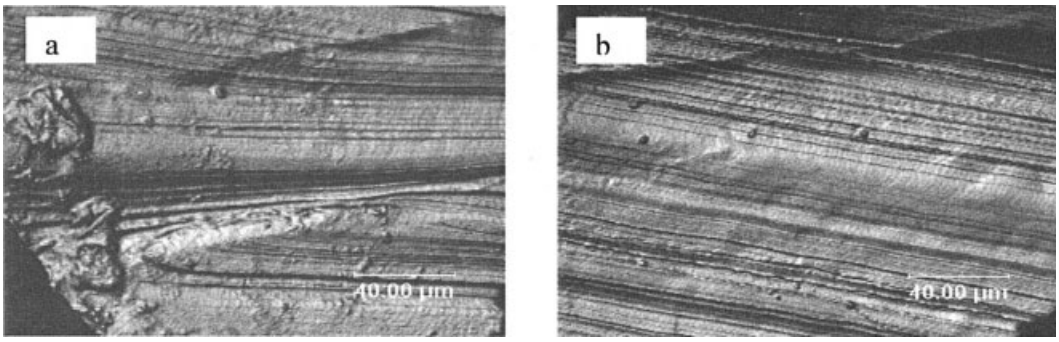

Figure 13 Micrographs of PA6 at 240°C and 184 KPa at: (a) periphery, (b) core.

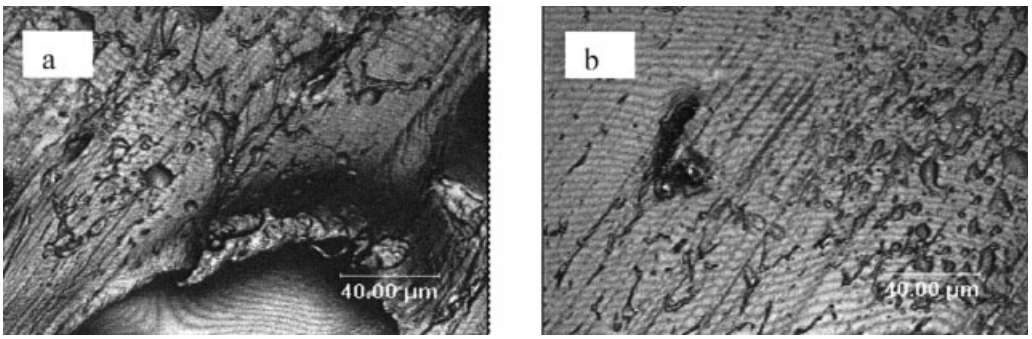

Figure 14 Micrographs of S12 at 230°C and 184 KPa at: (a) periphery, (b) core.

tration, at the same temperature and shear stress. This phenomenon may be observed in Figures 14–16. In the core region, there was laminar flow, presenting striation morphology, with the omnipresent bundles of fibers dispersed in the matrix.

With an increase in temperature (when examined at the highest temperature of 240°C), the morphological presentation showed the appearance of voids, increasingly so at the wall when compared to the core region (Figs. 17 and 18). Likewise, at the lower temperature and shear rates, bundling at the wall increased with fiber length and weight concentration. The presence of voids might be due to the expansion of gas bubbles in the material and were not indicative of pulled-out fibers as is usual in other studies.[37] The study postulated that the presence of many small voids and broken fibers showed that fibers have been pulled out during the fracture process, indicating that the adhesion of fiber and matrix was weak.

At the highest shear rate of 490 KPa, even at the same fiber concentrations, the bundles were pushed to the wall, with the core still presenting a laminar flow, signified by the striations in the matrix (Figs. 19 and 20).

From the micrographs, the presence of matrix material among the fibers is noticeable. This indicated the possibility of the matrix to have penetrated the void regions in the bundle of fibers. Thus, a better interfacial adhesion between the fiber and the matrix is indicated. Paiva and Frollini have reported the same results for sugercane bagasse-reinforced phenolic and lignophenolic composites.[16]

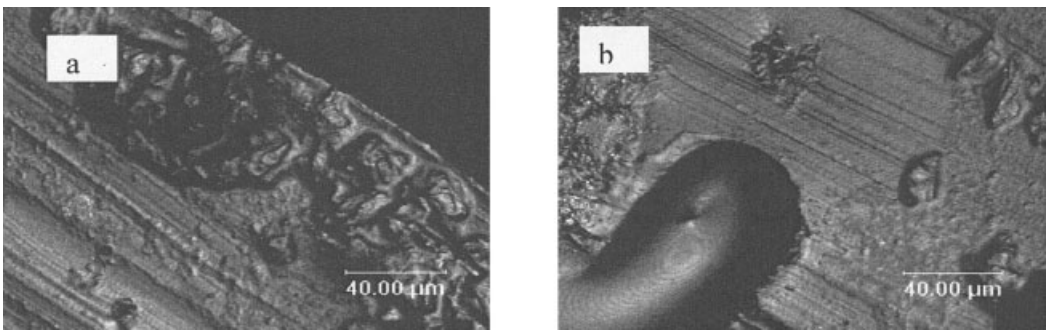

Figure 15 Micrographs of S110 at 230°C and 184 KPa at: (a) periphery, (b) core.

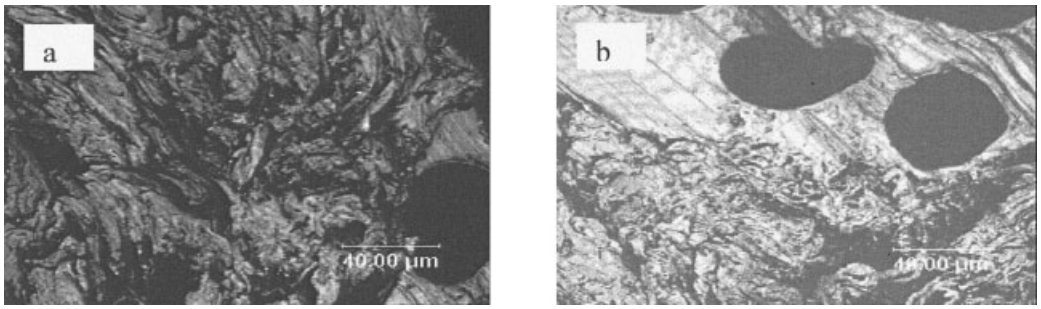

Figure 16 Micrographs of S310 at 230°C and 184 KPa at: (a) periphery, (b) core.

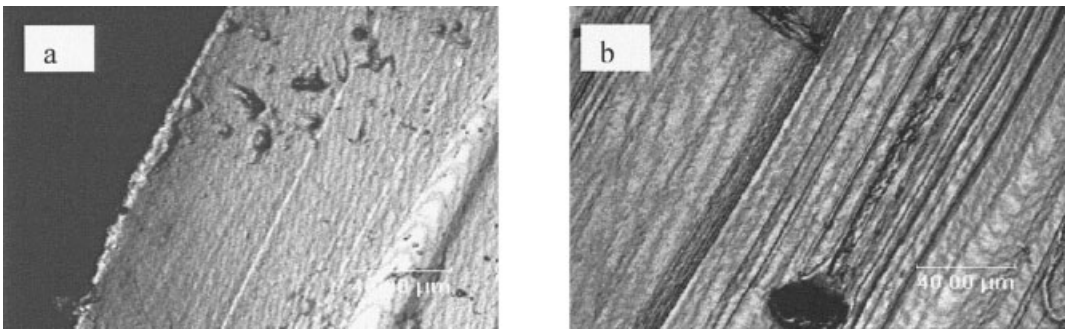

Figure 17 Micrographs of S110 at 240°C and 184 KPa at: (a) periphery, (b) core.

CONCLUSIONS

The thermal properties of the PA/bagasse blends were a function of crystallinity, and hence, PA content. With a decrease in PA content, the thermal properties likewise showed a decrease. It can be concluded it was possible to process the blends at the compositions studied without much deterioration in thermal properties, provided the shear rates are kept low. The PA/bagasse blends showed pseudoplastic behavior and obeyed the power-low equation. The viscosity of the blends increased with increasing fiber length and fiber content at low shear rate, but decreased below that of neat PA at high shear rates. The influence of fiber length and fiber loading is more pronounced at lower shear rate than at higher.

The viscosity of the blends was temperature sensitive and influenced by fiber length, particularly at higher temperatures. The addition of the fiber to the PA increased the activation energy, particularly at higher fiber lengths .The morphology of PA/bagasse showed the fibers to be randomly dispersed in the matrix, but the matrix presented the lamellar structure of polymer melts in a twin-screw extruder. There were changes observed according to the position where the melt was observed. In the core was laminar flow, with bundles of fiber dispersed in the matrix. An increase in temperature, showed voids, particularly so at the highest shear rates, but there appears to be smooth laminar flow in the center. It is therefore safe to assume that flow is slower at the wall, with bundles

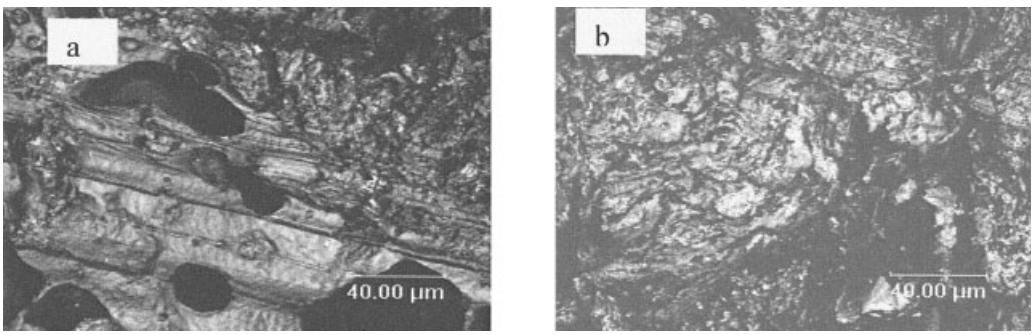

Figure 18 Micrographs of S110 at 240°C and 184 KPa at: (a) periphery, (b) core.

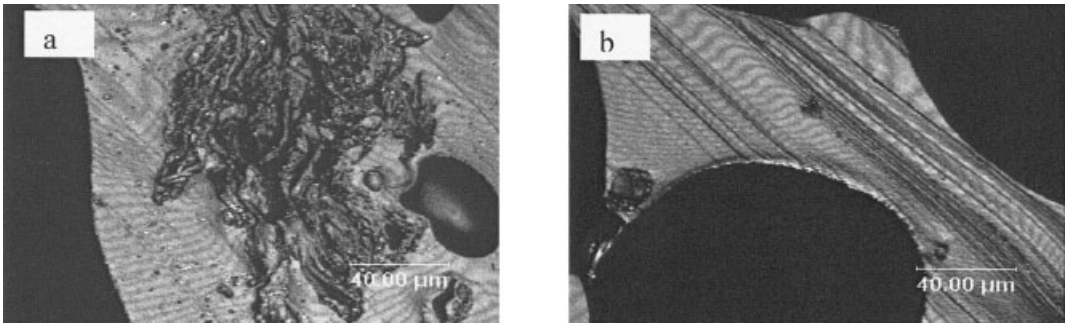

Figure 19 Micrographs of S15 at 230°C and 490 KPa at: (a) periphery, (b) core.

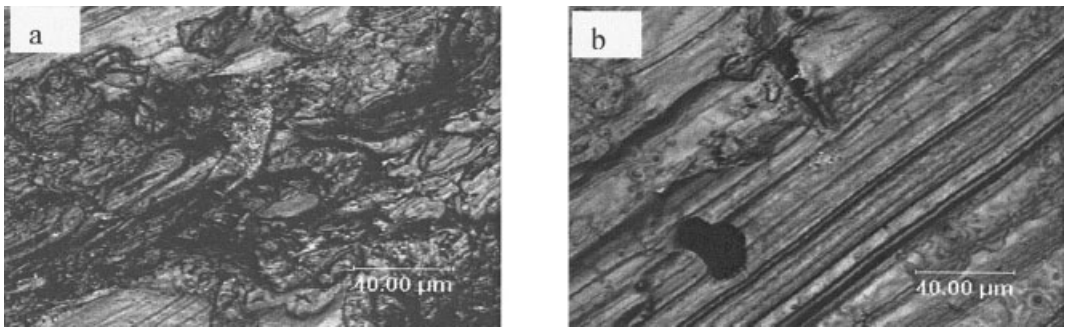

Figure 20 Micrographs of S35 at 230°C and 490 KPa at: (a) periphery, (b) core.

acting as flow resistors, but the flow patterns around the resistors need to be further studied.

The morphological studies of the flow phenomena is to help construct a material model of the melt such as that proposed by Van Krevelen[47] and Addinozio.[48] Based on our work, our material model of PA melt would be a melt with an advancing front curved inwards at the walls. The effect of reinforcement of this model would be to change the nature of the advancing front and the finer flow pattern.

References

1. Rozman, H. D.; Tay, G. S.; Tan, W. K.; Abubakar, A.; Kumar, R. N. Eur Polym 2001, 37, 1759.
2. Nair, K. C. M.; Diwan, S. M.; Thomas, S. J Appl Polym Sci 1996, 60, 1483.
3. Sanadi, A. R.; Caulfield, D. F.; Jacobson, R. E.; Rowell, R. M. Ind Eng Chem Res 1995, 34, 1889.
4. Thwe, M. M.; Liao, K. Composites 2002, 33, 43.
5. Rozman, H. D.; Tan, K. W.; Kumar, R. N; Abubakar, A.; Ishak, Z. A. M.; Ismail, H. Eur Polym 2000, 36, 1483.
6. Sanadi, A. R.; Caulfield, D. F.; Rowell, R. M. Plast Eng 1994, L (4), 27.
7. Ishak, Z. A. M.; Aminullah, A.; Ismail, H.; Rozman, H. D. J Appl Polym Sci 1998, 68, 2189.
8. Salyer, I. O.; Ball, G. L., III; Usmani, A. M.; Werkmeister, D. W. AID/US 1975, p. 31, 32, 190, 199.
9. Mclaughlin, E. C. J Mater Sci 1980, 15, 886.
10. Stael, G. C.; Tavares, M. I. B.; Almeida, J. R. M. Polym Test 2001, 20, 869.
11. Stael, G. C.; Tavares, M. I. B.; Almeida, J. R. M. Polym Polym Compos 2000, 8, 489.
12. Vazquez, A.; Dominguez, V. A.; Kenny, J. M. J Thermoplast Compos Mater 1999, 12, 477.
13. Hassan, M. L.; El-Wakil, N. A.; Sefain, M. Z. J Appl Polym Sci 2001, 79, 1965.
14. Hassan, M. L.; Rowell, R. M.; Fadi, N. A.; Yakoub, S. F.; Christainsen, A. W. J Appl Polym Sci 2000, 76, 561.
15. Bilba, K.; Arsene, M.-A.; Ouensanga, A. Cement Concrete Compos 2002.
16. Paiva, J. M. F.; Frollini, E. J Appl Polym Sci 2002, 83, 880.
17. Li, Y.; Mai, Y.-W.; Ye, L. Compos Sci Technol 2000, 60, 2037.
18. Deshpande, A. P.; Rao, M. B.; Rao, C. L. J Appl Polym Sci 2000, 76, 83.
19. Bledzki, A. K.; Gassa, J. Prog Polym Sci 1999, 24, 221.
20. Leao, A. L.; Rowell, R.; Tavares, N. Science and Technology of Polymers and Advanced Materials; Plenum Press: New York, 1998, p 755.
21. Wu, S. H.; Wang, F. Y.; Ma, C. C. M.; Chang, W. C.; Kuo, C. T.; Kuan, H. C.; Chen, W. J. Mater Lett 2001, 49, 327.
22. Yu, Z.; Ait-Kadi, A.; Brisson, J. Polym Eng Sci 1991, 31, 1228.
23. Tanaka, H.; Watanabe, K. Polym Eng Sci 1999, 39, 817.
24. Huitric, J.; Mederic, P; Moan, M.; Jarrin, J. Polymer 1998, 39, 4849.
25. Cimmino, S.; Coppola, F.; D'Orazio, L.; Greco, R.; Maglio, G.; Malinconico, M.; Mancarella, C.; Martuscelli, E.; Ragosta, G. Polymer 1986, 27, 1874.
26. Liang, B.-R.; White, J. L.; Sprueili, E.; Goswami, C. J Appl Polym Sci 1983, 28, 2011.
27. Aoki, Y.; Watanabe, M. Polym Eng Sci 1992, 32, 878.
28. Li, X.; Chen, M.; Huang, Y.; Cong, G. Polym Eng Sci 1999, 39, 881.
29. Varlet, J.; Perez, J.; Vassoille, R.; Vigier, G.; Glotin, M.; Cavaille, J. Y. J Mater Sci 1993, 28, 5560.
30. Garcia-Ramirez, M.; Cavaille, J. Y.; Dupeyre, D.; Peguy, A. J Polym Sci Polym Phys 1994, 32, 1437.
31. Garcia-Ramirez, M.; Cavaille, J. Y.; Dufresne, A.; Tekely, P. J Polym Sci Part B Polym Phys 1995, 33, 2109.
32. Garcia-Ramirez, M.; Cavaille, J. Y.; Dufresne, A.; Dupeyre, D. J Appl Polym Sci 1996, 59, 1995.
33. Nishio, Y.; Manley, R. S. J Polym Eng Sci 1990, 30, 71.
34. Mwaikambo, L.Y.; Ansell, M. P. J Appl Polym Sci 2002, 84, 2222.
35. Afshari, M.; Kotek, R.; Kish, M. H.; Dast, H. N. D.; Gupta, B. S. Polym 2002, 43, 1331.
36. Poh, L. K; Zakaria, S.; Ahmed, S.; Abdullah, M.; Dahlan, K. Z. J Inst Mater Malaysia 2002, 3.
37. Zakaria, S.; Poh, L. K.; Ahmed, S.; Azhari, C. H., accepted.
38. Amash, A.; Zugenmaier, P. Polymer 2000. 41, 1589.
39. Nair, K. C. M.; Thomas, S.; Groeninckx, G. Compos Sci Technol 2001, 61, 2519.
40. Glasser, W. G.; Taib, R.; Jain, K.; Kander, R. J Appl Polym Sci 1999, 73, 1329.
41. Sreekala, M. S.; Kumaran, M. G.; Thomas, S. J Appl Polym Sci 1997, 66, 821.
42. Fuad, M. Y. A.; Zaini, M. J.; Jamaludin, M. Polym Test 1994, 13, 15.
43. Asaletha, R.; Kumaran, M. G.; Thomas, S. Polym Degrad Stabil 1998, 61, 431.
44. George, J.; Janardhan, R.; Anand, J. S.; Bhagawan, S. S.; Thomas, S. Polym 1996, 37, 5421.
45. Nair, K. C. M.; Kumar, R. P.; Thomas, S.; Schit, S. C.; Ramamurthy, K. Compos Part A 2000, 31, 1231.
46. Basu, D.; Banerjee, A. N.; Misra, A. J Appl Polym Sci 1992, 46,1999.
47. Van Krevelen, D. W. Properties of Polymers. Armsterdam: Elsevier, 1990.
48. Addonizio, M. L.; D'Orazio, L.; Mancarella, C.; Martuscelli, E.; Casale, A.; Filippi, A. J Mater Sci 1989, 24, 2939.